LIMNOLOGY and OCEANOGRAPHY

ASLO

Limnol. Oceanogr. 9999, 2022, 1–14

doi: 10.1002/lno.12271

Light and hydrologic connectivity drive dissolved oxygen synchrony in stream networks

Jacob S. Diamond [1*] **Gilles Pinay** [2] **Susana Bernal** [3] **Matthew J. Cohen** [4] **David Lewis** [5] **Anna Lupon** [3] **Jay Zarnetske** [6] **Florentina Moatar** [1]

[1]RiverLy, INRAE, Centre de Lyon-Grenoble Auvergne-Rhône-Alpes, Lyon, France
[2]Environnement, Ville & Société (EVS UMR5600), Centre National de la Recherche Scientifique (CNRS), Lyon, France
[3]Integrative Freshwater Group, Centre for Advanced Studies of Blanes (CEAB-CSIC), Blanes, Spain
[4]School of Forest, Fisheries and Geomatics Sciences, University of Florida, Gainesville, Florida
[5]Department of Integrative Biology, University of South Florida, Tampa, Florida
[6]Department of Earth and Environmental Sciences, Michigan State University, East Lansing, Michigan

Abstract

Stream dissolved oxygen (DO) dynamics are an outcome of metabolic activity and subsequently regulate ecosystem functions such as in-stream solute and sediment reactions. The synchronization of DO signals in and across stream networks is both a cause and effect of the mode and timing of these functions, but there is limited empirical evidence for network patterns of DO synchrony. We used high frequency DO measurements at 42 sites spanning five catchments and stream orders to evaluate DO signal synchrony in response to variation in light (a driver of photosynthesis) and discharge (a control on DO signal spatial extent). We hypothesized that stream network DO synchrony arises when regional controls dominate: when light inputs are synchronous and when longitudinal hydrologic connectivity is high. By complement, we predicted that DO signal synchrony decreases as light becomes more asynchronous and stream flows decline or become discontinuous. Our results supported this hypothesis: greater DO signal synchrony arose with increasing light synchrony and flow connectivity. A model including these two controls explained 70% of variation in DO synchrony. We conclude that DO synchrony patterns within- and across-networks support the current paradigm of discharge and light control on stream metabolic activity. Finally, we propose that DO synchrony patterns are likely a useful prerequisite for scaling subdaily metabolism estimates to network and regional scales.

Synchrony of environmental variation is increasingly used to understand how ecosystems (Larsen et al. 2021; Seybold et al. 2021) and catchments (Abbott et al. 2018; Van Meter et al. 2020) function. However, using observations of synchrony to inform our understanding of ecosystem function remains a challenge. In streams, the fundamental processes of primary productivity and respiration (i.e., "ecosystem metabolism") lead to predictable daily rhythms of dissolved oxygen (DO). These rhythms are regularly measured at reach scales to quantify stream quality, energy and elemental budgets (Odum 1956; Heffernan and Cohen 2010; Appling et al. 2018*b*), and are useful indicators of many ecosystem processes (Diamond et al. 2021). Hence, patterns of DO synchronization among reaches may indicate temporal alignment of stream network processes, and thus provide insight into whole network functions.

The inherent advective flow and hierarchical structure of stream networks results in a gradient of physical conditions that may predict the spatial scales of DO synchrony (e.g., Vannote et al. 1980). Indeed, the upstream length over which a DO signal is derived—the "integration length"—is a function of stream physical attributes (depth, velocity, temperature) that control both gas exchange and advective transport (Chapra and Di Toro 1991; Hensley et al. 2018). At low flow, longitudinal flow connectivity that transports signals downstream is reduced, leading to reduction in integration lengths (Ward et al. 2018). The resulting patchy network structure can desynchronize DO signals as they are increasingly driven by varying local reach conditions (Dodds et al. 2018), stream intermittency (Sarremejane et al. 2022),

*Correspondence: jacob.diamond@inrae.fr

Additional Supporting Information may be found in the online version of this article.

Author Contribution Statement: Conceptualization: J.S.D., G.P., S.B., M.J.C., A.L., J.Z., and F.M. Methodology: J.S.D., G.P., and D.L. Software: J.S.D. Formal analysis: J.S.D. Investigation: J.S.D., G.P., and D.L. Data curation: J.S.D. Writing – original draft: J.S.D, G.P., S.B., M.J.C., A.L., and J.Z. Writing – review and editing: J.S.D., G.P., S.B., M.J.C., D.L., A.L., J.Z., and F.M. visualization: J.S.D. Supervision: G.P. and F.M. Funding acquisition: F.M. Project administration: F.M.

and discontinuities in source-water mixing (Ward and Stanford 1983). In contrast, higher flows increase integration lengths and longitudinal connectivity, smoothing heterogeneity in underlying processes and synchronizing DO signals along the network. Hence, DO synchrony among reaches may indicate network longitudinal connectivity, even as metabolism varies spatially in response to local drivers.

Regional phenomena like open-sky insolation and temperature can also synchronize network DO by imposing synchronous patterns of metabolic drivers (i.e., energy availability; Koenig 2002; Vogt et al. 2011). For example, a shared solar energy signal may induce the same diel productivity timing (and thus increase in diel DO) throughout a network, and even across networks in the same region (and same time zone). However, reach-scale properties can modify this shared forcing, leading to local variation in subdaily timing and magnitude of energy delivery to the stream ecosystem (Wu and Loucks 1995; Poole 2002). Indeed, local light availability varies with riparian shading (Mulholland et al. 2001; Savoy and Harvey 2021), topographic shading (Yard et al. 2005; Julian et al. 2008), stream azimuth (Savoy and Harvey 2021), and attenuation through the water column (Julian et al. 2008; Kirk et al. 2021). Hence, network DO synchrony likely arises when energy to drive productivity is uniformly delivered, and by contrast, DO synchrony diminishes when energy availability is local (Fig. 1).

It is important to note that DO signals can be synchronous (i.e., temporally aligned), despite having large variability in their daily amplitudes. There is therefore a key difference in spatial patterns of DO variation that inform network metabolic magnitude (Diamond et al. 2021 and references therein), vs. patterns of DO synchrony that inform metabolic timing. This notion of metabolic timing is a critical component toward extending our understanding of "metabolic regimes" from the reach scale (Bernhardt et al. 2018, 2022) to the network (Koenig et al. 2019) and from the subdaily rhythms of DO variation to patterns over decades.

In this study, we explored the seasonal patterns and drivers of DO synchrony across stream networks to test the following hypotheses. (1) Flow connectivity increases DO synchrony in a river network (Fig. 1, *x*-axis) because signal advection and mixing smooth heterogeneities in environmental drivers of stream metabolism such as light. (2) Light synchrony increases DO synchrony in a river network (Fig. 1, *y*-axis) because productivity-induced DO signals at sites within a catchment—or catchments within a region—are controlled by the timing of light reaching the stream surface. We expected light to be most spatially uniform during leaf-off periods (early spring and fall). We thus predicted that DO synchrony would decrease in summer when flow connectivity decreases and riparian canopies increase spatial heterogeneity in the timing of light delivery to the stream. To address this question and hypotheses, we considered both synchrony across all sites, regardless of stream network position or catchment membership, as well as synchrony among flow-connected sites (i.e., those where water from one site can flow to another; Larsen et al. 2021). The synchrony of these contrasting stream reach populations informs the relative importance of shared regional drivers vs. local drivers on downstream DO signal propagation.

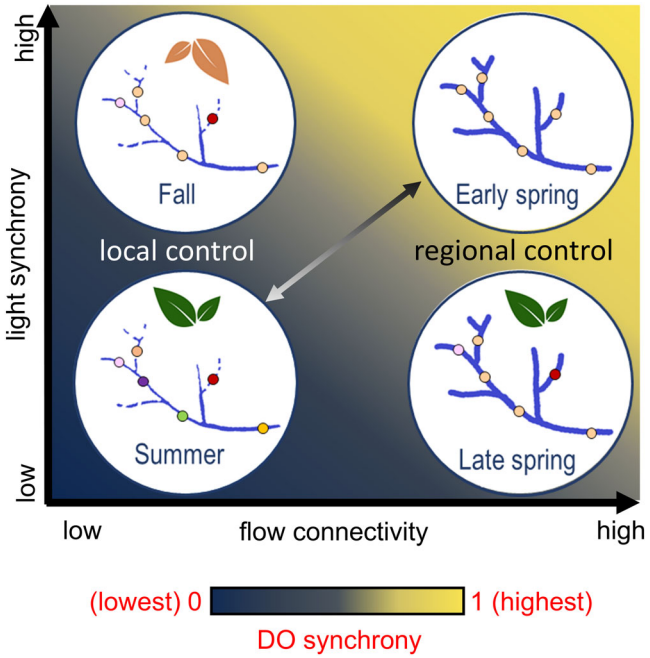

Fig. 1. Conceptual framework for dissolved oxygen (DO) synchrony (i.e., phase alignment of diel DO variation) across a stream network in response to temporal regimes of light and flow. Spatially homogenous timing of light delivery and high flow connectivity (e.g., typical in early spring in temperate catchments) are expected to increase DO synchrony (light shading). In contrast, DO synchrony declines under more spatially heterogeneous light regimes (e.g., riparian leaf-on) and/or when summertime stream intermittency reduces flow connectivity (dashed lines in stream network). Sites (filled circles in the network) of the same color indicate synchronous behavior and different colors indicate asynchronous behavior.

Methods

Study area

We studied 42 stream sites ranging from Strahler order 1 to 5 within five agricultural headwater catchments in the Forez region (~ 2000 km^2) of the Loire River, France from July 2019 to October 2020 (Fig. 2), with 4, 11, 16, 8, and 3 sites in orders 1–5, respectively. Granite and gneiss lithology at upper catchment boundaries gradually gives way to thick alluvium with clay and sand at catchment outlets in a flat basin known as the Forez plain. Sites span an elevation gradient of 330–627 m.a.s.l. (NGF IGN69 datum) and the regional topography is characterized by rolling hills with successions of plateaus separated by long, steep slopes. Climate is continental,

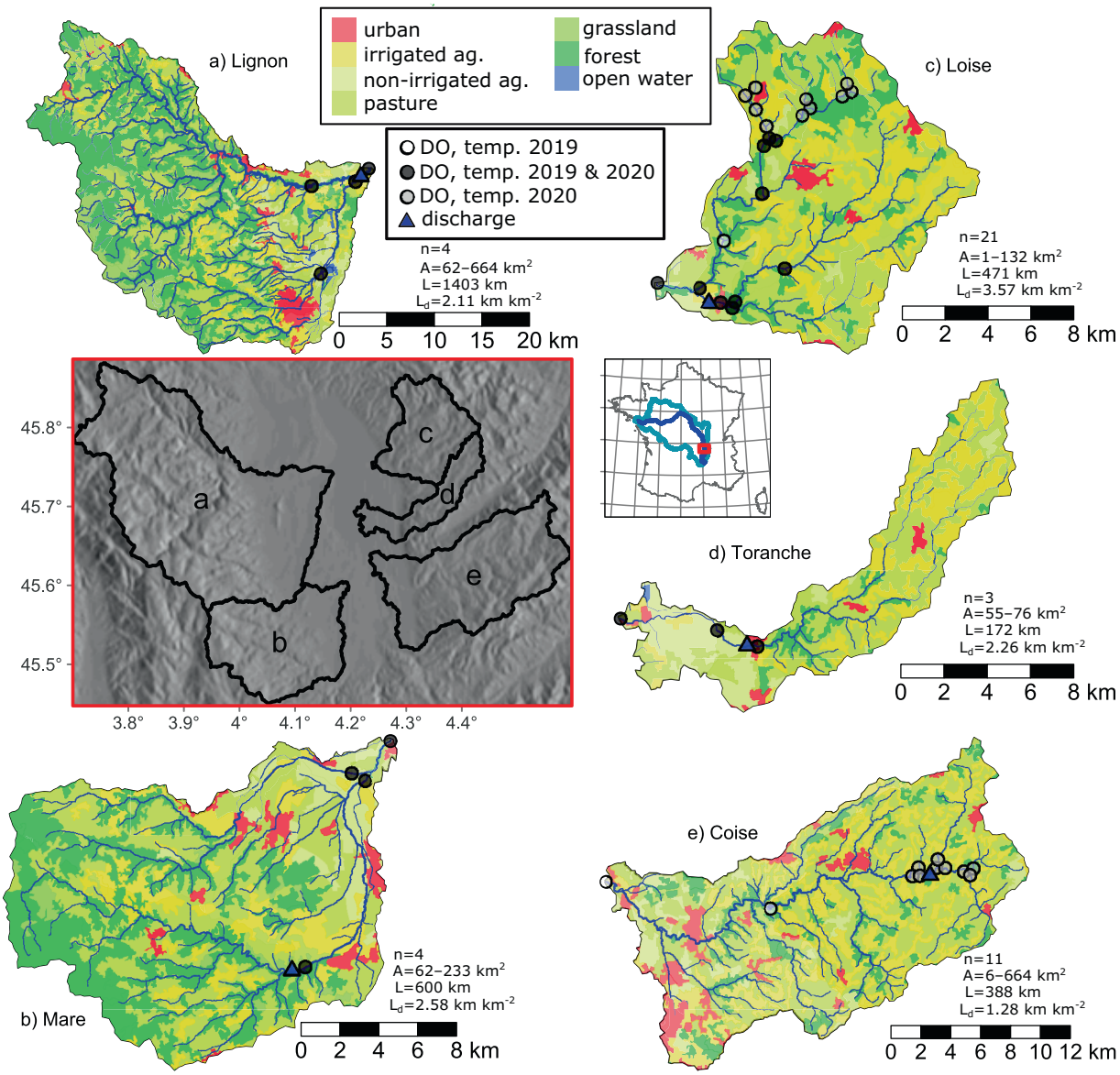

Fig. 2. Map of the 42 stream sites measured for DO and water temperature. Sites spanned five catchments in the headwaters (large inset) of the Loire River, France (small inset; Loire River basin in light blue). Corinne land cover classes shown for each catchment. Stream sites symbols are shaded according to the timing and length of the measurement period for DO. Discharge measurement sites are shown with blue triangles. Text indicates number of sites in each catchment (*n*), range of site catchment areas (*a*), total catchment stream length (*L*), and mean catchment stream density (L_d).

with mean annual rainfall of 800 mm, and mean annual temperatures of 11°C (range during measurement period = 0.0–34.3°C). The area has been under continuous agricultural activity over the last 2000 years (Georges et al. 2004) and recent intensive agricultural practices have led to high nutrient surpluses (e.g., 30 kg N ha^{-1} yr^{-1}; 10 kg P ha^{-1} yr^{-1}) (Diamond et al. 2021; Moatar et al. 2021). Additional consequences of this long agricultural history include dam, water mill, and weir infrastructure throughout the river network (Cubizolle et al. 2003, 2012; Georges et al. 2004), particularly in the Coise catchment.

Data collection and processing

We monitored all sites (Fig. 2) for DO (mg L^{-1}) and stream temperature (°C) between July 2019 and October 2020, but not during winter (November–February). In 2020, we began data collection on 3 March for sites in the eastern catchments (Fig. 2c–e), and on 7 June for sites in the western catchments that were largely comprised of Strahler orders 4 and 5 (Fig. 2a,b). At each site, DO and stream temperature were measured every 15 min with an in situ sensor (HOBO U26-001; Onset Computer Corporation, MA) instrumented with a copper anti-biofouling guard. We cleaned DO sensors

every 2 weeks to remove biofouling. Prior to deployment, we lab-calibrated DO sensors with both 100% water-saturated air and with sodium sulfite for 0% saturation. We also measured DO and temperature with a calibrated handheld probe (Pro Plus; YSI Inc., OH) at each field visit to check for sensor drift and develop corrections as needed. We placed sensors in the middle of the water column, and as close to the thalweg as possible. The sensor sites downstream of confluences were placed at least 20 stream widths downstream of the confluence to ensure mixing (Siders et al. 2017). These sites were also placed to minimize the potential influence of additional downstream tributaries.

For calculations of longitudinal hydrologic connectivity, light availability, and DO saturation, we gathered meteorological and hydraulic data from several sources, described in detail in Diamond et al. (2021). These data include hourly atmospheric pressure (kPa), open-sky insolation ($W\ m^{-2}$), daily mean discharge (Q; $m^3\ s^{-1}$), specific discharge (q; $mm\ d^{-1}$), stream depth (m), water velocity (v; $m\ s^{-1}$), and wetted channel width (m) for each site. We assumed spatially constant q within each catchment, allowing us to extrapolate Q at each measurement point (Fig. 2, blue triangles) to our sites based on their associated drainage area. Using site-scaled Q, we modeled stream depth, width, and v from an empirical reach-based hydraulic geometry model with high accuracy and low bias for our study region (Morel et al. 2020; Diamond et al. 2021). We further obtained an hourly shade factor (unitless) for each site using a previously developed shade factor model for the Loire basin (Loicq et al. 2018; Seyedhashemi et al. 2022). The shade factor varies between 0, indicating full light at the stream surface, and 1, indicating complete shade. We calculated hourly light for each site by multiplying open-sky insolation by the complement of the site-specific shade factor.

We applied a series of quality controls to DO data prior to analysis. Briefly, we (1) averaged 15-min data to hourly resolution to reduce file sizes and processing time, (2) removed data that were extremely noisy, collected in dry conditions, or otherwise of suspect quality, and (3) corrected for sensor drift. For hourly data that passed quality control (n_{DO} = 195,720), we calculated hourly DO equilibrium saturation (DO_{eq}) using water temperature and barometric pressure at sea level corrected for site elevation with the Garcia–Gordon model (Garcia and Gordon 1992). Additional detail on these quality controls are described in Diamond et al. (2021). For all subsequent analyses, we used the relative percentage DO saturation ($DO_{sat} = 100 \times DO/DO_{eq}$) to control for regional drivers of pressure and temperature. Finally, to reduce the effects of instrument noise on subsequent synchrony analyses, which can be considerable (Fig. S1), we smoothed all hourly time series with a 2nd order lowpass Butterworth digital filter (critical frequency = 0.24) using the *butter()* function from the *signal* R package (signal developers 2013).

Data analyses

Synchrony in DO, light, and temperature

We calculated the synchrony of hourly DO_{sat}, temperature, and light at the stream surface using the Kuramoto order parameter, r (Kuramoto 1975), which permits simultaneously analyzing many oscillators (i.e., sites) (Acebrón et al. 2005). Throughout, we used stream temperature synchrony as a reference point for synchrony in DO_{sat} and light. Given N oscillators, each with an instantaneous phase θ_j in a complex plane, r is the magnitude of their average vector $\mathbf{z}$ with average phase ψ (Fig. 3):

$$re^{i\psi} = \overline{\mathbf{z}} = \frac{1}{N}\sum_{j=1}^{N} e^{i\theta_j}$$

when $r = 1$, the phases of all N oscillators are identical (i.e., perfect synchrony), whereas when $r = 0$, the phases are distributed evenly around a complex plane circle (i.e., perfect

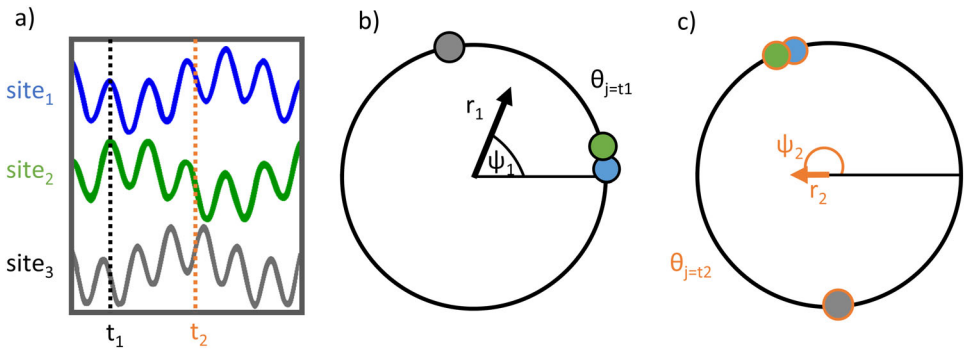

Fig. 3. Time series of three sites with the geometric interpretations of their Kuramoto order parameter, r, at two times, t_1 and t_2. (**a**) Time series for each site is colored and presented with arbitrary y-axis values and continuous time on the x-axis; it is clear that $site_1$ and $site_2$ behave more synchronously than $site_3$. The instantaneous phases, θ_j, of the three sites are shown for (**b**) t_1 and (**c**) t_2 as likewise colored points on the unit circle. Their average vector is given by the complex number $re^{i\psi}$, shown as an arrow. At t_1 the sites are more synchronous than they are at t_2, which is indicated by the magnitude of the vector, $\boldsymbol{r}$.

asynchrony). Hereafter, we operationally use "synchrony" to refer to r.

The Kuramoto approach is a valuable complement to Pearson correlations widely used in the synchrony literature (Koenig 2002; Pace and Cole 2002; Zanon et al. 2019), and it requires less computation than wavelet analyses (Sheppard et al. 2017, 2019). Moreover, the Kuramoto order parameter is useful in that it estimates instantaneous synchrony, not aggregate synchrony at time steps longer than the unit of measurement, which would otherwise be invisible with classical correlations analyses. Wavelet analyses also provide such detail, and may be appropriate diagnostics of synchrony when multiple time scales are of interest (Walter et al. 2017, 2021).

We measured θ_j of each hourly time series using the Hilbert transform from the *ifreq()* function in the R package *seewave* (Sueur et al. 2008). Prior to analysis, we detrended and z-scored each time series using the *cleandat()* function in the *wsyn* package (Reuman et al. 2021). We further linearly interpolated missing data with a maximum gap of 6 h (0.7% of all data); data gaps greater than 6 h were not filled. Synchrony calculations require no missing data so sites with missing data were not included in analysis. To minimize this information loss, we analyzed the data in weekly time steps so that even if a site was removed due to a data gap in a particular week (e.g., due to drying), it could still be included in analyses for other weeks. Subweekly approaches would have been just as valid, but increased computer processing time, and data gaps were typically at least 1 week in length. The number of sites used in each weekly synchrony analysis ranged from 7–35 (mean ± SD; 28 ± 5), 22–35 (29 ± 4), and 10–29 (22 ± 6) for stream temperature, light, and DO_{sat}, respectively. Weeks with the least sites were in summer 2020 when many low-order streams held no flowing surface water. Overall, we analyzed the following number of hourly data points for DO_{sat} (n = 195,720) temperature (n = 223,436), and light (n = 111,737, only calculated for daylight hours). Despite a varying number of sites throughout the analysis period, we observe that r is robust to this variation, in particular when analyzing more than 10 sites (Fig. S2).

To test our hypotheses, we calculated synchrony (i.e., r) for two site groupings: (1) across all sites, regardless of catchment or Strahler order, and (2) between flow-connected sites. In general, large phase differences among sites are required to substantially affect r, especially when analyzing many sites (Fig. S2), such that values less than 0.8 indicate relatively high asynchrony among sites. For flow-connected sites, synchrony was measured in pairwise fashion for all possible site pairs ($n_{pairs} \leq 112$) in any given week. For this analysis, r indicates the instantaneous phase difference between two sites: a value of 1 indicates in-phase, a value of 0 indicates anti-phase, a value of 0.7 indicates a 90° phase shift, a value of 0.5 indicates a 120° phase shift (for perfect sinusoids). In the context of paired site analysis, a consistent 90° or 120° phase shift between sites could indicate that the time difference between diel DO_{sat} maxima (or minima) is 6 or 9 h, respectively. Overall, the all sites analysis allowed us to evaluate regional synchrony in DO_{sat} signals, highlighting the time-varying effect of light synchrony. By complement, the flow-connected (site pairs) analysis allowed us to quantify the importance of along-network signal smoothing on DO_{sat} synchrony.

Calculating flow connectivity

To determine flow connectivity between sites, we first calculated a site-specific daily DO integration length, L_{DO}, [L], which is the upstream length of influence for the measured DO signal. We chose the term "DO integration length" over the previously used "DO footprint" (cf. Demars et al. 2015) because a "footprint" has two dimensions, whereas our focus is the along-channel linear dimension. DO signals at a point are most strongly influenced by processes occurring just upstream, with exponentially declining influence with distance upstream.

The L_{DO} depends on v [L T^{-1}], which controls the downstream translation of a DO signal, and the atmospheric gas exchange coefficient, K [T^{-1}], which controls how quickly that signal is erased (Chapra and Di Toro 1991; Demars et al. 2015). We describe L_{DO} as the distance at which 5% of the upstream DO signal persists (i.e., $3v/K$). Both v and K are time varying, and depend of stream hydraulics and temperature. We calculated K as the temperature-dependent (i.e., Schmidt number-corrected) and depth-corrected value of the standardized gas transfer velocity, k_{600} (Wanninkhof 1992), which we estimated as the average of four empirical equations (eqs. 1, 3, 4, and 5 in table 2 of Raymond et al. 2012) that depend on our daily estimates of stream geometry and hydraulics (Diamond et al. 2021).

We then calculated the ratio between the daily L_{DO} for each downstream site of a flow-connected pair and the channel length distance to the upstream site, d_{site}, [L]. This (dimensionless) connectivity ratio ($C = L_{DO}/d_{site}$) was used as a proxy of flow connectivity. When the connectivity ratio is large ($C \gg 1$), the DO diel signal at the upstream site directly influences the signal at the downstream site through signal advection. In contrast, when the connectivity ratio is small ($C < 1$), synchrony between DO diel signals is not driven by signal advection. The C between any two sites will change as temperature, v, and K change.

Hypotheses testing

We evaluated our hypotheses in two ways. First, we created a heatmap of our synchrony estimates to visually compare with Fig. 1, allowing us to map the influence of—and interaction between—flow connectivity (using C) and light synchrony (using the light synchrony r parameter). We expected that light synchrony was the most important control on the temporal alignment of primary productivity across sites and therefore the synchrony of DO_{sat} signals. This is distinct from homogeneity in light magnitude to the stream benthos, which should primarily control the magnitude of primary productivity (Kirk et al. 2021), and thus the amplitude of diel

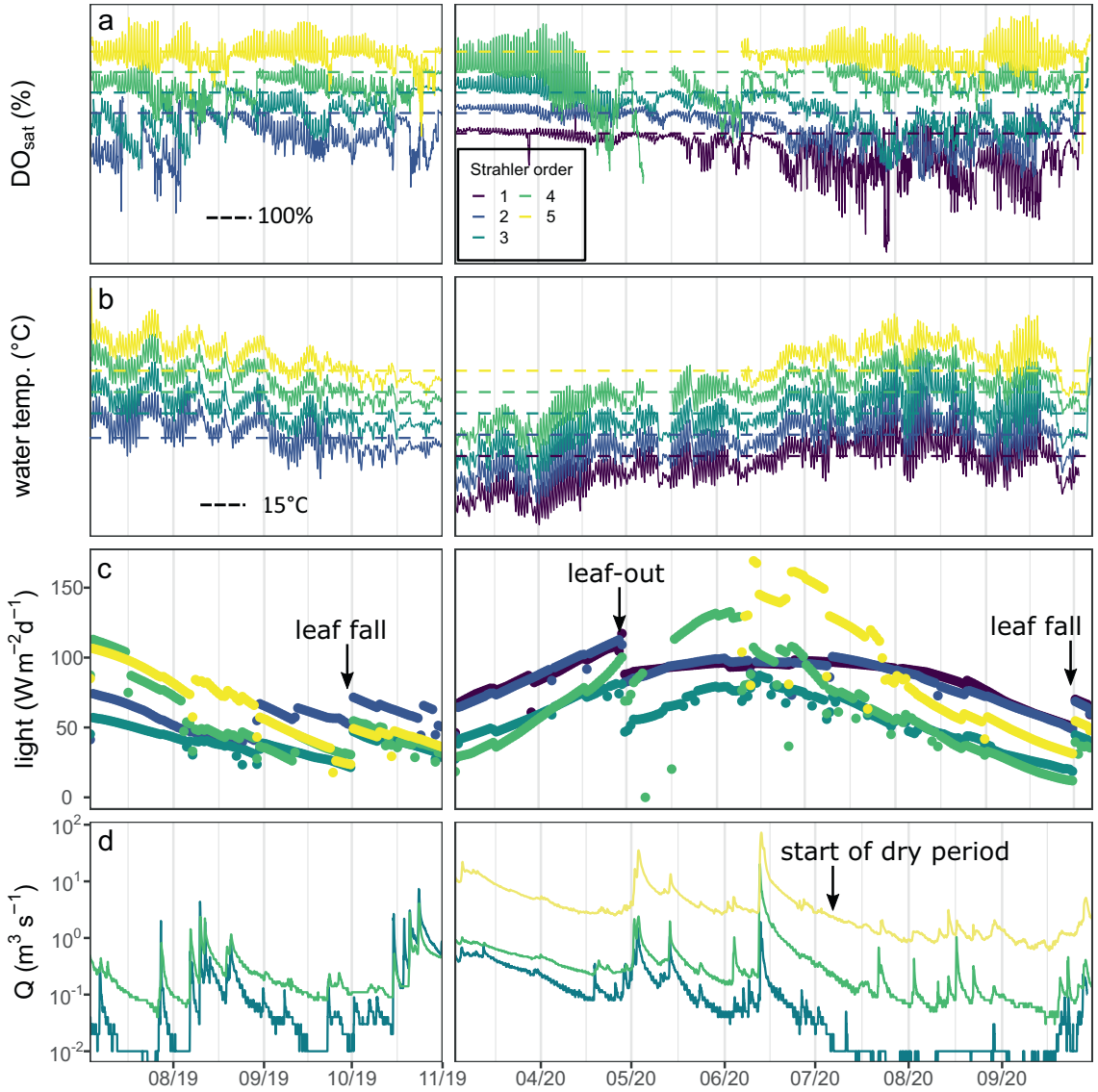

Fig. 4. Time series of (**a**) hourly mean DO$_{sat}$, (**b**) hourly mean stream temperature, (**c**) daily light at the stream surface, and (**d**) hourly mean discharge of all sites grouped by Strahler order, indicated with different colors. There are 4, 11, 16, 8, and 3 sites, respectively, within orders 1–5 in panels **a–c**. (**d**) Three discharge records representative of 3rd–5th order stream flow conditions in the study region are shown; note log scale of discharge. To enhance visualization, note for DO$_{sat}$ in (**a**) and temperature in (**b**) that values for each Strahler order are vertically shifted to minimize overlapping and obscuring of data, but all data share the same relative scale, which is shown with a reference dashed line representing 100% saturation for DO$_{sat}$ (**a**) and 15°C for temperature (**b**). Gaps in data indicate missing data or sensor failure.

DO$_{sat}$ signals (Diamond et al. 2021). To clarify, we measured the phase of signals, not their magnitude.

One of the predictions from our hypothesis that flow connectivity increases DO$_{sat}$ synchrony is that synchrony between flow-connected sites with low C (i.e., $C < 1$) should be similar to the mean synchrony of flow-unconnected sites. In other words, when $C < 1$, the upstream site is not sharing DO information with the downstream site and their synchrony should be indistinguishable from two unconnected sites. We evaluated this prediction directly by comparing the daily mean synchronies of all flow-connected sites to flow-unconnected sites as a function of C. There were 1347 unique pairs of flow-unconnected sites compared to the 112 unique pairs of flow-connected sites for this analysis. For $C < 1$, these synchronies should be statistically equivalent, but for $C > 1$, the flow-connected synchronies should be greater than flow-unconnected synchronies. Therefore, for a given site, on day d we calculated (1) C with a flow-connected upstream site, (2) its DO$_{sat}$ synchrony with a flow-connected upstream site, and (3) its mean DO$_{sat}$ synchrony with every unconnected site. We then compared its flow-connected and mean flow-unconnected synchrony across its

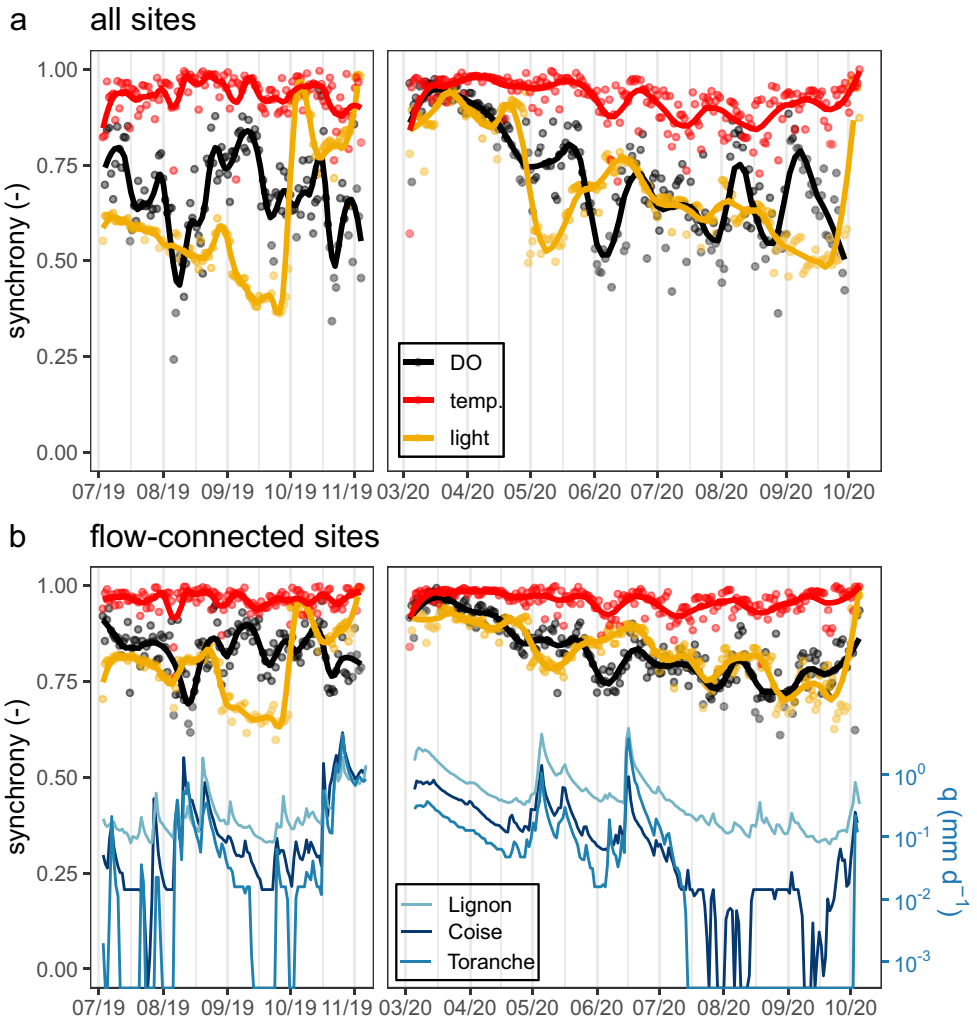

Fig. 5. Temporal evolution of daily mean synchrony (*r*, Kuramoto parameter; dimensionless) of hourly signals for 42 sites across five catchments. A synchrony value of 1 means perfect synchrony and a value of 0 means complete asynchrony. (**a**) Synchrony of all sites evaluated together for DO_{sat} (black), stream temperature (red), and light (gold). (**b**) Mean DO_{sat} synchrony between all flow-connected site pairs ($n = 112$), with specific discharge (q) for three contrasting catchments shown in blue on a log scale for reference of the hydrologic state of the catchments. Dots indicate daily means and loess lines show general trends (span of loess lines = 0.15 on $n = 80$).

range of C, and simplified these visually with generalized additive models.

As a second test of our hypotheses, we used a multiple regression model to quantify the relationships between DO_{sat} synchrony and both light synchrony and C. The model considered DO_{sat} synchrony as the dependent variable and light synchrony, C, and their interaction as predictors (Eq. 1). We developed a parallel model with temperature as the dependent variable to provide a benchmark for interpreting patterns observed for DO_{sat} (Eq. 2). We did so with the prediction that temperature synchrony would be more independent of light synchrony and flow connectivity than DO_{sat} because its temporal signal is primarily driven by regional air temperature patterns (Seyedhashemi et al. 2021, 2022) and because heat transport lacks the rapid erasure due to gas exchange that controls, and shortens, the DO signal. Hence, larger fitted effect sizes for DO_{sat} than for temperature provide additional support that light synchrony (through its control on primary productivity) and flow connectivity (through its control on signal integration) drive DO_{sat} synchrony. For these two multiple regressions, for each day, there were 112 possible upstream–downstream site pairs, each with a different C and pair-specific r for light, temperature, and DO_{sat}. There were overall 12,840 site-pair-day combinations. To reduce both temporal autocorrelation effects and inflated F-statistics from the large sample size, we performed the regressions on binned data. We binned the data into $n = 100$ percentiles of the natural log C ($\ln C_i$ for $i = 1$–100) as it was log-normally distributed, and subsequently calculated mean $\bar{r}_i$ for DO_{sat}, light, and temperature among the

128 observations within each percentile bin. All analyses were conducted in R (R Core Team 2020).

$$\bar{r}_{\mathrm{DO},i} = \beta_{0,\mathrm{DO}} + \beta_{1,\mathrm{DO}}\bar{r}_{\mathrm{light},i} + \beta_{2,\mathrm{DO}}\ln C_i + \beta_{3,\mathrm{DO}}\left(\bar{r}_{\mathrm{light},i}\ln C_i\right), \quad (1)$$

$$\bar{r}_{\mathrm{temp},i} = \beta_{0,\mathrm{temp}} + \beta_{1,\mathrm{temp}}\bar{r}_{\mathrm{light},i} + \beta_{2,\mathrm{temp}}\ln C_i + \beta_{3,\mathrm{temp}}\left(\bar{r}_{\mathrm{light},i}\ln C_i\right). \quad (2)$$

Results

Temporal patterns in DO and its drivers

All physiochemical variables varied greatly both within and among sites. Across Strahler orders, diel variation in DO_{sat} and stream temperature increased throughout March and April 2020, prior to the leaf out of riparian vegetation (Fig. 4a,b) as light availability at the water surface increased (Fig. 4c). At the end of April–early May 2020, vegetation leaf out occurred (Fig. 4c), coinciding with several storm events that increased discharge across all catchments (Fig. 4d). The combination of these two factors corresponded to reduced diel amplitudes (Table S1) and apparent desynchronization of DO_{sat} (Fig. 4a) and stream temperature (Fig. 4b) across orders. In July, stream flow began to decline dramatically across all orders, but was most pronounced for Strahler order 3 (Fig. 4d). Between July and mid-September 2020, 32 sites ceased flowing at least once, with lower-order sites, particularly in the eastern catchments, remaining dry for periods as long as 1 month (Fig. 4d). There was clear variation in the timing of light inputs across Strahler orders (Fig. 4c), and light timing was even more variable across sites.

Synchrony in diel signals of DO, light, and temperature

Overall, synchrony of stream temperature ($r = 0.94 \pm 0.10$; mean ± SD) was higher than synchrony of DO_{sat} ($r = 0.73 \pm 0.20$) and light ($r = 0.68 \pm 0.22$), with stream temperature nearly perfectly synchronous ($r > 0.9$) across all 42 sites for most of the study. DO_{sat} and light exhibited a similar seasonal pattern, where synchrony was nearly perfect (i.e., $r = 1$) in early spring, but decreased over late spring and summer (Fig. 5a), though this pattern was more evident in 2020 than in 2019. In fall, light synchrony clearly increased, but DO_{sat} synchrony was largely unchanged from late spring and summer. When evaluated only within flow-connected sites, synchrony of all variables increased (Fig. 5b); yet stream temperature ($r = 0.95 \pm 0.15$) was more synchronous than light ($r = 0.84 \pm 0.25$) and DO_{sat} ($r = 0.83 \pm 0.25$). Outside of the vernal window, DO_{sat} r values among flow-connected sites indicate mean phase differences in DO signals between 6 and 9 h.

Example time series from the Loise catchment demonstrate how hourly synchrony across stream orders varied among contrasting periods of light synchrony and flow connectivity (Fig. 6a–d). During early spring, before leaf-out, with relatively synchronous light across the five catchments (Fig. 5) and high flow connectivity ($q = 0.18$ mm d^{-1}; $C \geq 1$; Fig. S3), the DO_{sat} signals from the nine sites within the Loise catchment were highly synchronous (Fig. 6b), with synchrony dipping slightly near solar noon. In contrast, synchrony in DO_{sat} was markedly lower just a month later, after leaf-out, despite similar discharge ($q = 0.21$ mm d^{-1}; Fig. 6d). In this case, the general synchrony pattern inverted, with synchrony peaking near solar noon (Fig. 6d). Later in the summer, when flow connectivity decreased ($q = 0.01$ mm d^{-1}) and incident light was asynchronous, DO_{sat} synchrony was lowest. During this period, DO_{sat} peaked at low-order sites in the mid-morning, whereas the DO_{sat} maxima occurred later in the day for higher order sites (Fig. 6c). During similar low flow connectivity conditions in October 2019 ($q = 0.03$ mm d^{-1}), at the onset of leaf fall when light was more synchronous, DO_{sat} synchrony exhibited a similar diel pattern as in early spring, but with a pronounced dip in the afternoon (Fig. 6a). Across the study period, the lowest DO_{sat} synchrony ($r < 0.5$) predominately occurred at night (62%), with the mode of low synchrony occurring between 00:00 h and 01:00 h. In contrast, the highest synchrony ($r > 0.9$) predominately occurred during the day (66%), with the mode of high synchrony occurring between 12:00 h and 13:00 h.

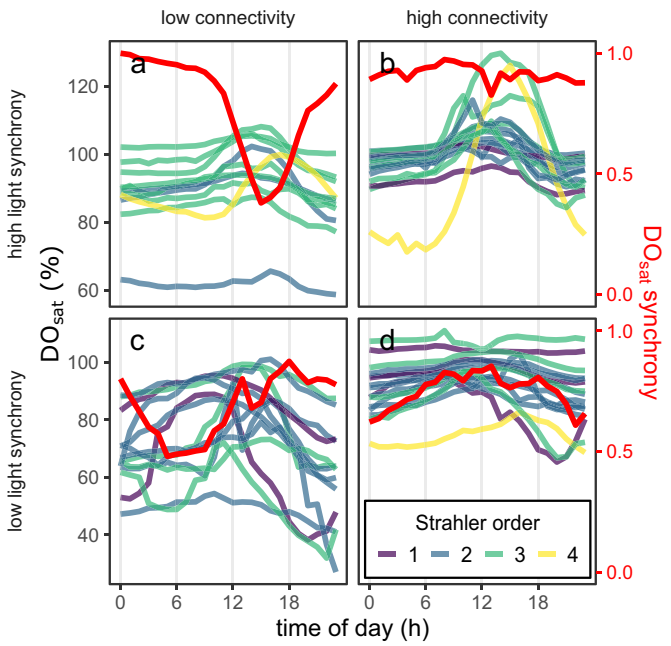

Fig. 6. Hourly time series of DO_{sat} and their synchrony. Each panel is 1 d from four contrasting periods resulting from the interaction of light spatial variability at the stream surface and flow connectivity similar to scenarios depicted in Fig. 1. Each time series comes from sites in the Loise catchment (n = 9, 16, 9, 16, respectively, for **a–d**) colored by their Strahler order. Shown in red (secondary y-axis) is the hourly synchrony of these time series calculated with the Kuramoto order parameter, r. the four periods correspond to: (**a**) early autumn in a dry year (2019-10-14); (**b**) springtime before leaf-out (2020-04-11); (c) late summer in a dry year (2020-07-14); (**d**) springtime after leaf-out (2020-05-18).

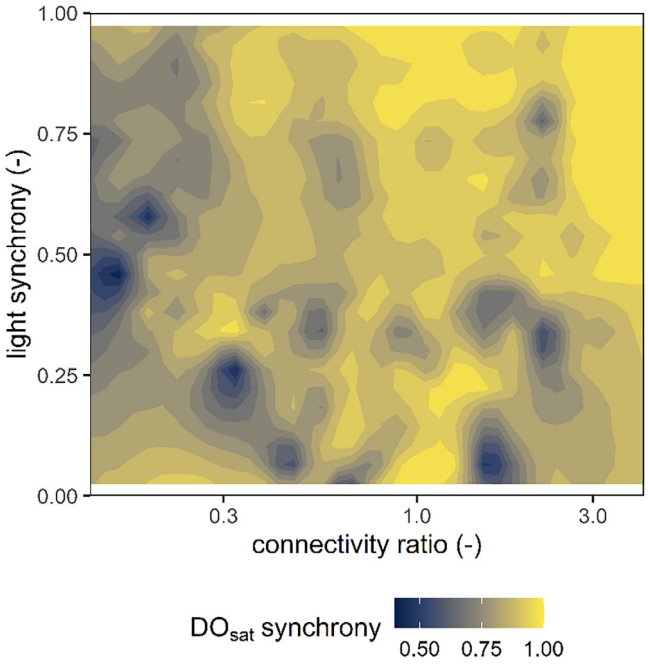

Fig. 7. Synchrony in DO_{sat} as a function of light synchrony and flow connectivity (measured as connectivity ratio). All hourly data from the paired synchrony analysis (n = 14,717) were plotted according to light synchrony and C, and then colored according to DO_{sat} synchrony, with yellow and blue colors indicating high and low synchrony, respectively. To improve visualization and to allow direct comparison with our hypothesized scenarios in Fig. 1, both axes were then binned into 20 equally spaced bins (note log scale on x-axis) and mean values of DO_{sat} synchrony were calculated and then smoothed with ordinary kriging.

Spatiotemporal patterns in longitudinal flow connectivity

L_{DO} were highly dynamic across sites during the study period, often varying by an order of magnitude between high and low flow conditions (Fig. S3a,b). Across all sites, L_{DO} spanned four orders of magnitude, from 50 to 55,000 m (mean ± SD = 2000 ± 3900 m), but was typically less than the mean distance between flow-paired sites, d_{site} (6615 ± 3312 m; range = 108–20,770 m). L_{DO} was highly variable within each Strahler order, with Strahler orders 2–4 (35 of 42 sites) exhibiting the greatest variability. Strahler orders 1–2 had L_{DO} < 100 m during late spring and summer, while values for Strahler order 4–5 were regularly > 1 km. Connectivity ratios, C, were thus also temporally and spatially variable (Fig. S3c), ranging from 0.02–10.34 (1.18 ± 1.34). Strahler orders 2–4 exhibited similar C ranges (0.1–2) and medians (0.5), whereas values for Strahler order 5 were nearly an order of magnitude greater (Fig. S3d). For Strahler order 2, C rarely exceeded 1 during late spring and summer, but for Strahler order 3, C was commonly greater than 1 during the same period (Fig. S3c).

Light synchrony and hydrological connectivity as drivers of DO_{sat} synchrony

Synchrony in DO_{sat} was positively related to flow connectivity and light synchrony (Fig. 7) in line with our predictions. DO_{sat} synchrony increased with increasing flow connectivity, and was clearly lower when $C < 1$ for Strahler order 2–4 (Fig. S4a). We likewise observed general increases in DO_{sat} synchrony with increases in light synchrony both across sites (Fig. S5a) and between connected sites (Fig. S5b). Generally, stream temperature synchrony was also positively related to C, but the relationship was weaker than for DO_{sat} (lower slope) for Strahler orders 2–4, likely because temperature was highly synchronous at all C (Fig. S4b). Moreover, DO_{sat} synchrony between weakly flow-connected sites ($C < 1$) was indistinguishable from synchrony between flow-unconnected sites, while synchrony between strongly flow-connected ($C > 1$) sites was much higher than synchrony between flow-unconnected sites (Fig. S6).

Models explaining DO and temperature synchronies further quantified the strength of light synchrony and C effects. The multiple regression model with an interaction of mean daily light synchrony and mean daily C (binned into 100 percentiles) explained 70% of the variance in mean daily DO_{sat} synchrony (Table 1; variance inflation factor = 1.15). The model indicates that flow connectivity and light synchrony effects on DO_{sat} synchrony are of similar magnitude and influence DO_{sat} synchrony in the same direction. The positive interaction indicates that either of these factors boosts the influence of the other on DO_{sat} synchrony. In other words, high flow connectivity between sites synchronizes their DO_{sat}

Table 1. Multiple regression results for mean daily DO_{sat} and temperature synchrony.

	DO_{sat} ($F_{96,3}$ = 76.48)		Temperature ($F_{96,3}$ = 62.84)	
Term	**Estimates***	**p†**	**Estimates***	**p†**
(Intercept)	0.85±0.0032	**<0.001**	0.96±0.00094	**<0.001**
Light synchrony	0.024±0.0035	**<0.001**	0.0057±0.0010	**<0.001**
ln(C)	0.028±0.0035	**<0.001**	0.0082±0.0010	**<0.001**
Light synchrony: ln(C)	0.014±0.0023	**<0.001**	−0.00082±0.00068	0.228
R^2_{adj}	0.70		0.65	

Models relate DO_{sat} and temperature synchrony to the C, light synchrony, and their interaction, using 100 equally spaced bins of ln(C).
*Values were centered and scaled before regression and values indicate mean ± standard error.
†p Values less than 0.01 are bolded.

values, but does so more dramatically when the sites have similar light availability. While the model for temperature synchrony explained a similar proportion of the variance as did the model for DO_{sat} synchrony (65%), the fitted slopes were far smaller, likely due to the much higher intercept (0.96) compared to DO_{sat} (0.85; Table 1). These results indicate that temperature had high synchrony, regardless of light synchrony or C.

Discussion

We observed clear support for our conceptual model (Fig. 1) hypothesizing that diel DO synchrony in headwater networks is driven by both the spatiotemporal variation in longitudinal flow connectivity and light synchrony (Fig. 7, Table 1). Critically, flow-connected sites were consistently more synchronous than non flow-connected sites, despite considerable diel signal erasure between sites. Results here demonstrate that network-scale diel DO synchrony predictably emerges through a balance between energetic drivers of metabolism and hydraulic drivers of signal transport and smoothing operating at multiple scales.

Measuring high-resolution synchrony

Overall, our approach to quantify synchrony in and across stream networks revealed how stream networks generate and transmit DO signals, and enabled the assessment of spatiotemporal heterogeneity previously hidden by lower frequency sampling. Indeed, most environmental synchrony studies examine effects at seasonal and interannual scales (Baines et al. 2000; Kling et al. 2000; Van Meter et al. 2020). In contrast, the Kuramoto order parameter allowed the evaluation of synchrony at hourly scales (Fig. 6) across and within catchments; and is worth noting as a potentially useful tool in future ecological synchrony studies. With this tool, we were able to observe increasing DO synchrony during the day, implying that signals are aligned by sunlight, but then diverge when that forcing ceases. We could also see inverted patterns of reduced daytime synchrony when signal smoothing was low (e.g., Fig. 6a). This is likely induced from a downstream increase in K that prolongs the timing of DO peaks and lengthens diel DO recession shape. Channel transient storage and stream depth also alter diel DO signal geometry (Hensley and Cohen 2016), leading to predictable downstream network patterns of DO—and other solute—synchrony. Although we conducted our analyses at daily scales (because flow connectivity was only available at the daily scale), future work exploring environmental synchrony at the same temporal scale as measurement may better reveal the network-scale timing and coupling of solute transport and transformation.

Terrestrial control on stream DO synchrony

The dual drivers of light and longitudinal connectivity on DO synchrony reflect two facets of riparian vegetation: leaf phenology and evapotranspiration. First, riparian leaf phenology controls light inputs to the stream, and thus, patterns of light synchrony. The period before vegetation sets leaves out for photosynthesis—approximately 1 May in the study region (Lebourgeois et al. 2008), is associated with limited riparian shading from vegetation, and corresponded to a period of high DO synchrony. Once leaves were out, however, temporal variability in local light delivery arose, which led to patchy network of temporally divergent primary productivity signals—supported by observed decreases in DO synchrony. We again note our focus here is on the synchrony of light availability, not on its magnitude, which is important for primary productivity and DO variation (Savoy et al. 2019; Diamond et al. 2021; Kirk et al. 2021). Second, riparian evapotranspiration can further contribute to decreases in DO synchrony throughout the growing season by reducing streamflow (Lupon et al. 2016) and longitudinal hydrological connectivity among reaches. Moreover, the influence of riparian evapotranspiration on streamflow grows as discharge decreases (Bond et al. 2002; Cadol et al. 2012), suggesting an increasing effect of riparian vegetation on hydrologic connectivity patterns over the growing season. These observations provide additional motivation to study terrestrial–aquatic connections within riparian corridors (Hynes 1975; Pinay et al. 2018), including the synchrony of their productivity (Bernhardt et al. 2018; Mejia et al. 2019; Walter et al. 2021) and respiration regimes (Bertuzzo et al. 2022).

Ecological implications of DO synchrony

DO signals within and across stream networks in the Loire headwaters synchronized under shared light synchrony and hydrological signal smoothing. This result is not surprising given that light and flow are the two major controls of stream metabolic activity (Bernhardt et al. 2022). However, we suggest that patterns of DO synchrony can provide additional insights into stream network functioning within and across catchments. For example, synchrony in networks of DO sensors could be used to evaluate the degree of hydrologic connectivity of ungauged networks, as our results indicate the two are strongly linked—indeed connectivity of sites is a much better predictor of synchrony than distance, alone (Fig. S7). However, our focus on advective transport and signal smoothing may not be the only mechanism linking flow connectivity to DO synchrony. Indeed, even at $C = 1$, which implies 95% signal loss between sites, we observed high DO_{sat} synchrony, even under asynchronous light conditions. Moreover, our results demonstrate that at $C < 1$ (e.g., 0.1–0.5; Fig. S6), corresponding to signal loss between stations near 100%, connected sites are more synchronous than disconnected sites. This result points to alternative explanations for how connectivity leads to synchrony. Perhaps most obvious is that high flow may induce similar environmental conditions for respiration and productivity across the network such that high connectivity is not so much smoothing variation among hotspots, but instead imposing common metabolism throughout. Regardless, the clear link between flow connectivity and

DO synchrony suggests their coupling and given the relative ease of DO sensor installation vis-à-vis hydrologic stations, perhaps there is utility in using DO sensor networks to estimate hydrologic conditions.

Our results also have implications for modeling stream metabolism at stream network scales. As DO datasets grow (e.g., Appling et al. 2018*b*) and demand increases for stream metabolism estimates (Bernhardt et al. 2018), researchers will need to be careful about their assumptions when scaling site level estimates to networks, catchments, and regions (Koenig et al. 2019; Diamond et al. 2021; Segatto et al. 2021). Modern metabolism methods rely on (at least) two key assumptions that our work adds nuance to: (1) a direct link between discharge and gas exchange, and (2) a link between peak primary productivity and solar noon. First, we clearly show that discharge is not just a critical component that controls (Raymond et al. 2012) and constrains gas exchange estimates (Appling et al. 2018*a*), but it also drives the integration length of metabolic signal origins. Hence, when scaling estimates from reaches to networks, the orders-of-magnitude temporally variable L_{DO} that defines a DO signal reach is of clear importance and may confound traditional applications of "reaches" as the places between confluences (cf. Segatto et al. 2021). Second, we demonstrate that care must be taken when using insolation estimates (e.g., with latitude and longitude) or regional measurements to scale metabolism at network scales as local conditions demonstrably desynchronize the temporal availability of sunlight for primary productivity. Finally, we suggest that network scale DO synchrony, which can be evaluated at subdaily time scales, is a useful complement to metabolic measurements, which are typically constrained to daily time steps. As primary productivity is a direct function of temporal light patterns (Bernhardt et al. 2022), and respiration is likely dynamic with subdaily variation in temperature and oxygen (Demars et al. 2011), we envision studies of signal synchrony yielding new insights that deconvolve these signals. More broadly, improving our capacity to assess metabolic forcing at finer than daily time scales will enable new ways of thinking about and assessing the magnitude and resilience of biological functions at the scale of whole river networks.

Conclusions

Our work here produces four primary conclusions. First, synchrony in stream DO, temperature, and light can be high within and across regional headwater stream networks, with DO synchrony strongly driven by high flow connectivity and light synchrony at the stream surface. Hence, reduced-complexity models of subdaily DO and metabolism can probably be used during high flow periods with synchronous light conditions. In contrast, when environmental conditions are dominated by local factors (shading and variable flow connectivity), more complex models or more observation effort is needed. Second, flow-connected sites are consistently more synchronous than flow-disconnected sites even when the signal information passing between sites is small. Hence, common watershed attributes between flow-connected sites like geology, aspect, and land use may be important but poorly quantified controls on synchrony. Third, we identify riparian vegetation phenology as a strong control on the proximal drivers of DO synchrony, providing a further linkage to be explored between terrestrial and aquatic ecosystem metabolic coupling. Finally, the general concepts and findings of local vs. regional drivers of stream DO synchrony are adaptable to research investigating the causes and implications of stream network synchrony for other ecological conditions from nutrients and organic matter to metabolic processes.

Data availability statement

Code to replicate analyses is available at: https://github.com/jakediamond/DO_synchrony_headwaters. Data to replicate analyses is available at: http://www.hydroshare.org/resource/31c8b6409b9b4fa4a3aca7a085cda95d.

References

Abbott, B. W., and others. 2018. Unexpected spatial stability of water chemistry in headwater stream networks. Ecol. Lett. **21**: 296–308. doi:10.1111/ele.12897

Acebrón, J. A., L. L. Bonilla, C. J. P. Vicente, F. Ritort, and R. Spigler. 2005. The Kuramoto model: A simple paradigm for synchronization phenomena. Rev. Mod. Phys. **77**: 137–185. doi:10.1103/RevModPhys.77.137

Appling, A. P., R. O. Hall, C. B. Yackulic, and M. Arroita. 2018*a*. Overcoming equifinality: Leveraging long time series for stream metabolism estimation. J. Geophys. Res.: Biogeosci. **123**: 624–645. doi:10.1002/2017JG004140

Appling, A. P., and others. 2018*b*. The metabolic regimes of 356 rivers in the United States. Sci. Data **5**: 180292. doi:10.1038/sdata.2018.292

Baines, S. B., K. E. Webster, T. K. Kratz, S. R. Carpenter, and J. J. Magnuson. 2000. Synchronous behavior of temperature, calcium, and chlorophyll in lakes of northern Wisconsin. Ecology **81**: 815–825. doi:10.2307/177379

Bernhardt, E. S., and others. 2018. The metabolic regimes of flowing waters. Limnol. Oceanogr. **63**: S99–S118. doi:10.1002/lno.10726

Bernhardt, E. S., and others. 2022. Light and flow regimes regulate the metabolism of rivers. Proc. Natl. Acad. Sci. USA **119**: e2121976119. doi:10.1073/pnas.2121976119

Bertuzzo, E., and others. 2022. Respiration regimes in rivers: Partitioning source-specific respiration from metabolism time series. Limnol. Oceanogr. **67**: 2374–2388. doi:10.1002/lno.12207

Bond, B. J., J. A. Jones, G. Moore, N. Phillips, D. Post, and J. J. McDonnell. 2002. The zone of vegetation influence on baseflow revealed by diel patterns of streamflow and

vegetation water use in a headwater basin. Hydrol. Process. **16**: 1671–1677. doi:10.1002/hyp.5022

Cadol, D., S. Kampf, and E. Wohl. 2012. Effects of evapotranspiration on baseflow in a tropical headwater catchment. J. Hydrol. **462–463**: 4–14. doi:10.1016/j.jhydrol.2012.04.060

Chapra, S. C., and D. M. Di Toro. 1991. Delta method for estimating primary production, respiration, and reaeration in streams. J. Environ. Eng. **117**: 640–655. doi:10.1061/(ASCE)0733-9372(1991)117:5(640)

Cubizolle, H., A. Tourman, J. Argant, J. Porteret, C. Oberlin, and K. Serieyssol. 2003. Origins of European biodiversity: Palaeo-geographic signification of peat inception during the Holocene in the granitic eastern Massif Central (France). Landsc. Ecol. **18**: 227–238. doi:10.1023/A:1024444628509

Cubizolle, H., F. Fassion, J. Argant, C. Latour-Argant, P. Galet, and C. Oberlin. 2012. Mire initiation, climatic change and agricultural expansion over the course of the late-Holocene in the Massif Central mountain range (France): Causal links and implications for mire conservation. Quat. Int. **251**: 77–96. doi:10.1016/j.quaint.2011.07.001

Demars, B. O., and others. 2011. Temperature and the metabolic balance of streams. Freshw. Biol. **56**: 1106–1121. doi:10.1111/j.1365-2427.2010.02554.x

Demars, B. O. L., J. Thompson, and J. R. Manson. 2015. Stream metabolism and the open diel oxygen method: Principles, practice, and perspectives. Limnol. Oceanogr.: Methods **13**: 356–374. doi:10.1002/lom3.10030

Diamond, J. S., S. Bernal, A. Boukra, M. J. Cohen, D. Lewis, M. Masson, F. Moatar, and G. Pinay. 2021. Stream network variation in dissolved oxygen: Metabolism proxies and biogeochemical controls. Ecol. Indic. **131**: 108233. doi:10.1016/j.ecolind.2021.108233

Dodds, W. K., and others. 2018. Spatial heterogeneity and controls of ecosystem metabolism in a Great Plains river network. Hydrobiologia **813**: 85–102. doi:10.1007/s10750-018-3516-0

Garcia, H. E., and L. I. Gordon. 1992. Oxygen solubility in seawater: Better fitting equations. Limnol. Oceanogr. **37**: 1307–1312. doi:10.4319/lo.1992.37.6.1307

Georges, V., J. Verrier, and H. Cubizolle. 2004. Occupation humaine et dynamique fluviale de la Loire en Forez, du Néolithique à l'époque gallo-romaine (France, 42). Occupation, gestion et paléoenvironnement des plaines alluviales de l'âge du Fer à l'Antiquité, Presses Universitaires Franc-Comtoises, Annales Littéraires. Série Environnement, sociétés et archéologie **10**: 121e134.

Heffernan, J. B., and M. J. Cohen. 2010. Direct and indirect coupling of primary production and diel nitrate dynamics in a subtropical spring-fed river. Limnol. Oceanogr. **55**: 677–688. doi:10.4319/lo.2010.55.2.0677

Hensley, R. T., and M. J. Cohen. 2016. On the emergence of diel solute signals in flowing waters. Water Resour. Res. **52**: 759–772. doi:10.1002/2015WR017895

Hensley, R. T., M. J. Cohen, and J. W. Jawitz. 2018. Channel filtering generates multifractal solute signals. Geophys. Res. Lett. **45**: 11722–11731. doi:10.1029/2018GL079864

Hynes, H. B. N. 1975. The stream and its valley. Int. Ver. Theor. Angew. Limnol.: Verh. **19**: 1–15. doi:10.1080/03680770.1974.11896033

Julian, J. P., M. W. Doyle, and E. H. Stanley. 2008. Empirical modeling of light availability in rivers. J. Geophys. Res.: Biogeosci. **113**. doi:10.1029/2007JG000601

Kirk, L., R. T. Hensley, P. Savoy, J. B. Heffernan, and M. J. Cohen. 2021. Estimating benthic light regimes improves predictions of primary production and constrains light-use efficiency in streams and rivers. Ecosystems **24**: 825–839. doi:10.1007/s10021-020-00552-1

Kling, G. W., G. W. Kipphut, M. M. Miller, and W. J. O'Brien. 2000. Integration of lakes and streams in a landscape perspective: The importance of material processing on spatial patterns and temporal coherence. Freshw. Biol. **43**: 477–497. doi:10.1046/j.1365-2427.2000.00515.x

Koenig, W. D. 2002. Global patterns of environmental synchrony and the Moran effect. Ecography **25**: 283–288. doi:10.1034/j.1600-0587.2002.250304.x

Koenig, L. E., A. M. Helton, P. Savoy, E. Bertuzzo, J. B. Heffernan, R. O. Hall Jr., and E. S. Bernhardt. 2019. Emergent productivity regimes of river networks. Limnol. Oceanogr.: Lett. **4**: 173–181. doi:10.1002/lol2.10115

Kuramoto, Y. 1975. Self-entrainment of a population of coupled non-linear oscillators, p. 420–422. *In* H. Araki [ed.], International symposium on mathematical problems in theoretical physics, v. **30**. Springer. doi:10.1007/BFb0013365

Larsen, S., and others. 2021. The geography of metapopulation synchrony in dendritic river networks. Ecol. Lett. **24**: 791–801. doi:10.1111/ele.13699

Lebourgeois, F., J.-C. Pierrat, V. Perez, C. Piedallu, S. Cecchini, and E. Ulrich. 2008. Déterminisme de la phénologie des forêts tempérées françaises: étude sur les peuplements du réseau Renecofor. Rev. For. Française **60**: 323–343. doi:10.4267/2042/19767

Loicq, P., F. Moatar, Y. Jullian, S. J. Dugdale, and D. M. Hannah. 2018. Improving representation of riparian vegetation shading in a regional stream temperature model using LiDAR data. Sci. Total Environ. **624**: 480–490. doi:10.1016/j.scitotenv.2017.12.129

Lupon, A., S. Bernal, S. Poblador, E. Martí, and F. Sabater. 2016. The influence of riparian evapotranspiration on stream hydrology and nitrogen retention in a subhumid Mediterranean catchment. Hydrol. Earth Syst. Sci. **20**: 3831–3842. doi:10.5194/hess-20-3831-2016

Mejia, F. H., A. K. Fremier, J. R. Benjamin, J. R. Bellmore, A. Z. Grimm, G. A. Watson, and M. Newsom. 2019. Stream metabolism increases with drainage area and peaks asynchronously across a stream network. Aquat. Sci. **81**: 9. doi:10.1007/s00027-018-0606-z

Moatar, F., and others. 2021. The Loire River basin, p. 225–289. *In* K. Tockner, C. Zarfl, and C. Robinson [eds.], Rivers of Europe. Elsevier.

Morel, M., D. J. Booker, F. Gob, and N. Lamouroux. 2020. Intercontinental predictions of river hydraulic geometry from catchment physical characteristics. J. Hydrol. **582**: 124292. doi:10.1016/j.jhydrol.2019.124292

Mulholland, P. J., and others. 2001. Inter-biome comparison of factors controlling stream metabolism. Freshw. Biol. **46**: 1503–1517. doi:10.1046/j.1365-2427.2001.00773.x

Odum, H. T. 1956. Primary production in flowing waters. Limnol. Oceanogr. **1**: 102–117. doi:10.4319/lo.1956.1.2.0102

Pace, M. L., and J. J. Cole. 2002. Synchronous variation of dissolved organic carbon and color in lakes. Limnol. Oceanogr. **47**: 333–342. doi:10.4319/lo.2002.47.2.0333

Pinay, G., S. Bernal, B. W. Abbott, A. Lupon, E. Marti, F. Sabater, and S. Krause. 2018. Riparian corridors: A new conceptual framework for assessing nitrogen buffering across biomes. Front. Environ. Sci. **6**: 47. doi:10.3389/fenvs.2018.00047

Poole, G. C. 2002. Fluvial landscape ecology: Addressing uniqueness within the river discontinuum. Freshw. Biol. **47**: 641–660. doi:10.1046/j.1365-2427.2002.00922.x

R Core Team. 2020. R: A language and environment for statistical computing. R Foundation for Statistical Computing.

Raymond, P. A., and others. 2012. Scaling the gas transfer velocity and hydraulic geometry in streams and small rivers: Gas transfer velocity and hydraulic geometry. Limnol. Oceanogr. **2**: 41–53. doi:10.1215/21573689-1597669

Reuman, D. C., T. L. Anderson, J. A. Walter, L. Zhao, and L. W. Sheppard. 2021. wsyn: Wavelet approaches to studies of synchrony in ecology and other fields. https://cran.r-project.org/web/packages/wsyn/

Sarremejane, R., M. L. Messager, and T. Datry. 2022. Drought in intermittent river and ephemeral stream networks. Ecohydrology **15**: e2390. doi:10.1002/eco.2390

Savoy, P., A. P. Appling, J. B. Heffernan, E. G. Stets, J. S. Read, J. W. Harvey, and E. S. Bernhardt. 2019. Metabolic rhythms in flowing waters: An approach for classifying river productivity regimes. Limnol. Oceanogr. **64**: 1835–1851. doi:10.1002/lno.11154

Savoy, P., and J. W. Harvey. 2021. Predicting light regime controls on primary productivity across CONUS river networks. Geophys. Res. Lett. **48**: e2020GL092149. doi:10.1029/2020GL092149

Segatto, P. L., T. J. Battin, and E. Bertuzzo. 2021. The metabolic regimes at the scale of an entire stream network unveiled through sensor data and machine learning. Ecosystems **24**: 1792–1809. doi:10.1007/s10021-021-00618-8

Seybold, E. C., M. L. Fork, A. E. Braswell, J. R. Blaszczak, M. R. Fuller, K. E. Kaiser, J. M. Mallard, and M. A. Zimmer. 2021. A classification framework to assess ecological, biogeochemical, and hydrologic synchrony and asynchrony. Ecosystems **25**: 989–1005. doi:10.1007/s10021-021-00700-1

Seyedhashemi, H., F. Moatar, J.-P. Vidal, J. S. Diamond, A. Beaufort, A. Chandesris, and L. Valette. 2021. Thermal signatures identify the influence of dams and ponds on stream temperature at the regional scale. Sci. Total Environ. **766**: 142667. doi:10.1016/j.scitotenv.2020.142667

Seyedhashemi, H., J.-P. Vidal, J. S. Diamond, D. Thiéry, C. Monteil, F. Hendrickx, A. Maire, and F. Moatar. 2022. Regional, multi-decadal analysis on the Loire River basin reveals that stream temperature increases faster than air temperature. Hydrol. Earth Syst. Sci. **26**: 2583–2603. doi:10.5194/hess-26-2583-2022

Sheppard, L. W., P. C. Reid, and D. C. Reuman. 2017. Rapid surrogate testing of wavelet coherences. EPJ Nonlinear Biomed. Phys. **5**: 1. doi:10.1051/epjnbp/2017000

Sheppard, L. W., E. J. Defriez, P. C. Reid, and D. C. Reuman. 2019. Synchrony is more than its top-down and climatic parts: Interacting Moran effects on phytoplankton in British seas. PLoS Comput. Biol. **15**: e1006744. doi:10.1371/journal.pcbi.1006744

Siders, A. C., D. M. Larson, J. Rüegg, and W. K. Dodds. 2017. Probing whole-stream metabolism: Influence of spatial heterogeneity on rate estimates. Freshw. Biol. **62**: 711–723. doi:10.1111/fwb.12896

signal developers. 2013. signal: Signal processing.http://r-forge.r-project.org/projects/signal/

Sueur, J., T. Aubin, and C. Simonis. 2008. Seewave, a free modular tool for sound analysis and synthesis. Bioacoustics **18**: 213–226. doi:10.1080/09524622.2008.9753600

Van Meter, K. J., S. Chowdhury, D. K. Byrnes, and N. B. Basu. 2020. Biogeochemical asynchrony: Ecosystem drivers of seasonal concentration regimes across the Great Lakes Basin. Limnol. Oceanogr. **65**: 848–862. doi:10.1002/lno.11353

Vannote, R. L., G. W. Minshall, K. W. Cummins, J. R. Sedell, and C. E. Cushing. 1980. The river continuum concept. Can. J. Fish. Aquat. Sci. **37**: 130–137. doi:10.1139/f80-017

Vogt, R. J., J. A. Rusak, A. Patoine, and P. R. Leavitt. 2011. Differential effects of energy and mass influx on the landscape synchrony of lake ecosystems. Ecology **92**: 1104–1114. doi:10.1890/10-1846.1

Walter, J. A., L. W. Sheppard, T. L. Anderson, J. H. Kastens, O. N. Bjørnstad, A. M. Liebhold, and D. C. Reuman. 2017. The geography of spatial synchrony. Ecol. Lett. **20**: 801–814. doi:10.1111/ele.12782

Walter, J. A., R. Fleck, J. H. Kastens, M. L. Pace, and G. M. Wilkinson. 2021. Temporal coherence between lake and landscape primary productivity. Ecosystems **24**: 502–515. doi:10.1007/s10021-020-00531-6

Wanninkhof, R. 1992. Relationship between wind speed and gas exchange over the ocean. J. Geophys. Res.: Oceans **97**: 7373–7382. doi:10.1029/92JC00188

Ward, J. V., and J. A. Stanford. 1983. The serial discontinuity concept of lotic ecosystems, p. 29–42. *In* T. D. Fontaine III

and S. M. Bartell [eds.], Dynamics of lotic ecosystems. Ann Arbor Science Publishers.

Ward, A. S., N. M. Schmadel, and S. M. Wondzell. 2018. Simulation of dynamic expansion, contraction, and connectivity in a mountain stream network. Adv. Water Resour. **114**: 64–82. doi:10.1016/j.advwatres.2018.01.018

Wu, J., and O. L. Loucks. 1995. From balance of nature to hierarchical patch dynamics: A paradigm shift in ecology. Q. Rev. Biol. **70**: 439–466. doi:10.1086/419172

Yard, M. D., G. E. Bennett, S. N. Mietz, L. G. Coggins, L. E. Stevens, S. Hueftle, and D. W. Blinn. 2005. Influence of topographic complexity on solar insolation estimates for the Colorado River, Grand Canyon, AZ. Ecol. Model. **183**: 157–172. doi:10.1016/j.ecolmodel.2004.07.027

Zanon, J. E., P. de Carvalho, L. C. Rodrigues, and L. M. Bini. 2019. Potential mechanisms related to the spatial synchrony of phytoplankton is dependent on the type of data. Hydrobiologia **841**: 95–108. doi:10.1007/s10750-019-04009-y

Acknowledgments

This project was supported by The Loire-Bretagne Water Agency and the Rhône-Méditerranée-Corse Water Agency. J.D. was also supported by the EUR H2O'Lyon, French ANR-17-EURE-0018 grant. S.B. work was funded by the CANTERA (RTI2018-094521-B-100) and EVASIONA (PID2021-122817-NB-100) projects and a Ramon y Cajal fellowship (RYC-2017-22643) from the Spanish Ministry of Science, Innovation, and Universities and AEI/FEDER UE. A.L. was supported by the program Beatriu de Pinós, funded by the Government of Catalonia and the Horizon 2020 research and innovation program (BP-2018-00082). JPZ work was partially supported by US NSF awards (1846855, 1916567) and a fellowship from the Collegium - Lyon, Institute for Advanced Study.

Conflict of Interest

None declared.

Submitted 14 April 2022
Revised 06 September 2022
Accepted 04 November 2022

Associate editor: Robert O Hall